Evidence for the Effects of Swell and Unsteady Winds on Marine Wind Stress

WILLIAM M. DRENNAN, HANS C. GRABER, AND MARK A. DONELAN*

Rosenstiel School of Marine and Atmospheric Science, University of Miami, Miami, Florida

(Manuscript received 25 July 1997, in final form 24 August 1998)

ABSTRACT

Over the past four decades much effort has been directed toward determining a parameterization of the sea surface drag coefficient on readily measurable quantities, such as mean wind speed and atmospheric stability. Although such a parameterization would have obvious operational advantages, the considerable scatter present between experiments, or within any one experiment, indicates that it is not easily achievable. One likely candidate for much of the scatter is the underlying wave field. Unfortunately, few campaigns over the years have included spectral measurements of the waves. Among those that have, the results are inconclusive.

Here data are presented from the Surface Wave Dynamics Experiment and High Resolution Remote Sensing Program campaigns in which 3-m discus buoys were instrumented with K-Gill and sonic anemometers and complete motion packages to measure the direct (eddy correlation) stress and, concurrently, the directional ocean wave spectrum. These data are examined for the effects of swell on the drag coefficient. It is found that much of the scatter in the drag coefficient can be attributed to geophysical effects, such as the presence of swells or nonstationary conditions.

1. Introduction

The air–sea fluxes of momentum, heat, and mass are important input parameters for coupled ocean–atmospheric models. It is common to relate these quantities to better known mean quantities (wind speed, air and sea surface temperatures, etc.) through the so-called bulk relations. Here the fluxes are related to the mean quantities through bulk transfer coefficients. In the case of momentum transfer, we have

$$\tau = \rho C_{zN}(U_{zN} - U_s)^2, \tag{1}$$

where τ is the surface stress, ρ the air density, C_{zN} the drag coefficient at z meters in neutrally stratified conditions, U_{zN} the mean neutral z-meter wind speed, and U_s the surface drift speed, usually assumed to be zero. In a constant stress layer away from the thin viscous layer near the surface, turbulent transport dominates and the surface stress is given by

$$\tau = \rho u_*^2 = \rho[(-\overline{u'w'})^2 + (-\overline{v'w'})^2]^{1/2}, \tag{2}$$

where u', v', and w' are the turbulent fluctuations in the horizontal in-line, horizontal lateral, and vertical velocities, respectively, and the overbar refers to time averaging over a suitable period, typically 20 min in the near-surface boundary layer (Pierson 1983). The above serves as a definition for the friction velocity u_*.

Since the work of Smith (1980), it has been accepted that C_{10N}, the 10-m neutral drag coefficient, is dependent on the wind speed. Numerous results since then have supported this assertion [see Geernaert (1990) for a summary; see also Yelland and Taylor (1996)]. However, due to the considerable amount of scatter within individual experiments, and especially between experiments, no universally accepted relationship has emerged. Recent efforts have been focused on identifying and quantifying the effects of other physical parameters.

Donelan (1990), with subsequent support from Smith et al. (1992) and Donelan et al. (1992), has shown an additional dependence of C_{10N} on the development of the wave field, with C_{10N} increasing for younger wave ages. This corroborated the earlier work of Kitaigorodskii and Volkov (1965), who hypothesized that the surface roughness length z_o decreased with increasing wave age c_p/u_*, where c_p represents the phase speed of waves at the peak of the windsea spectrum. The drag coefficient and roughness length are related via

$$C_{zN} = \kappa^2[\log(z/z_o)]^{-2} \tag{3}$$

as readily follows from (1) and

* Additional affiliation: National Water Research Institute, Canada Centre for Inland Waters, Burlington, Ontario, Canada.

Corresponding author address: Dr. William M. Drennan, Division of Applied Marine Physics, Rosenstiel School of Marine and Atmospheric Science, University of Miami, 4600 Rickenbacker Causeway, Miami, FL 33149-1098.
E-mail: wdrennan@rsmas.miami.edu

$$U_{zN} = \frac{u_*}{\kappa} \log(z/z_o), \tag{4}$$

the logarithmic velocity profile of a constant stress layer, where the von Kármán constant κ is approximately 0.4. This dependence of C_{10N} on wave age has particular relevance in nearshore and intense storm regions where conditions are often fetch- or duration-limited. However, windseas on the open ocean are generally quite close to full development, making a wave age effect difficult to discern.

The presence of mixed windsea and swells has also been proposed as a factor influencing the drag coefficient. Using laboratory data Donelan (1987) showed a significant effect of gentle swells on the development of the windsea. In the field, Donelan et al. (1997) reported significantly enhanced drag coefficients in conditions where light winds opposed strong swells. These eddy-correlation ship data were supported by the near-simultaneous remotely sensed data of Nghiem et al. (1995), who observed significantly enhanced radar backscatter. However, Dobson et al. (1994) investigating the drag coefficient–wind speed relationship in conditions of pure windsea and windsea–swell combinations, did not find a statistically significant effect in the presence of swells. Unfortunately such a dependence is difficult to find in most existing datasets, especially offshore ones, due to the lack of concurrent wave data. Hence it is very difficult to determine if the high degree of scatter in existing datasets can be ascribed to properties of the wave or wind fields.

Mahrt et al. (1996) discuss several other possible sources of scatter in the drag coefficients, such as flux averaging time and vector versus scalar averaging, but conclude that these are significant primarily in weak wind events, typically $U < 3$ m s^{-1}.

We report here on an extensive dataset collected during the SWADE (Surface Wave Dynamics Experiment) and High-Res (High Resolution Remote Sensing Program) campaigns off the U.S. East Coast (Fig. 1). The data consist of nearly a thousand hours of eddy-correlation stress data and concurrent wave directional spectra collected from 3-m discus buoys and covering 15 strong wind ($U > 10$ m s^{-1}) events. With this unique dataset, we investigate the possible dependence of the wind stress (and drag coefficient) on the underlying wave field.

2. Modified 3-m discus buoys in SWADE and High-Res

The use of moving platforms for making eddy-correlation measurements dates from the 1960s, when systems for aircraft usage were developed (e.g., Miyake et al. 1970a). Although similar systems were developed for marine usage (e.g., Fujitani 1985), the cost of implementation remained prohibitive until the development of the latest generation of motion sensors. Since eddy-correlation techniques are critically dependent on

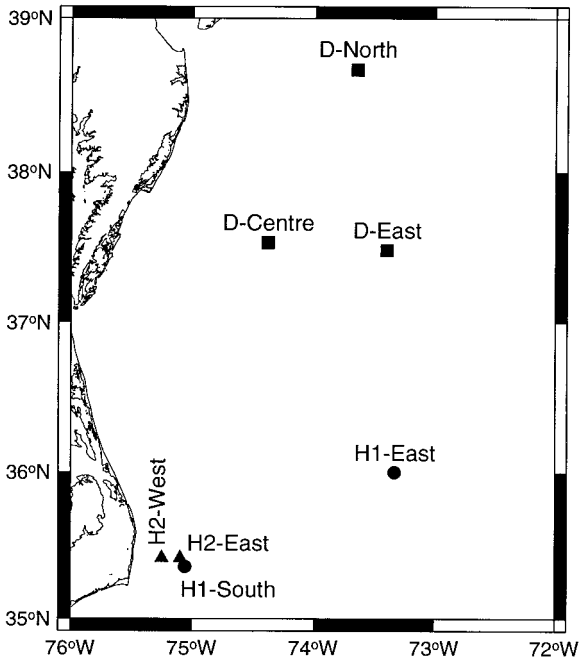

FIG. 1. Location map of the SWADE and High-Res experiments. The prefix ''D'' denotes the SWADE buoys, while H1 and H2 denote High-Res-I and High-Res-II, respectively.

the accurate measurement of the vertical velocity, their successful implementation from moving platforms demands that the full motion of the platform be recorded, and these signals used to correct the measured velocity signals—see below. Early attempts to make eddy-correlation measurements from ships or buoys (e.g., Mitsuta and Fujitani 1974; Bradley et al. 1991) are based on incomplete motion correction (i.e., not all degrees of motion were measured) and are therefore suspect except in very calm conditions. Only in the past few years, with the increased availability of small, inexpensive accelerometers and gyroscopes (or rate gyros), has it become feasible to use ships or buoys for direct flux measurements (see Katsaros et al. 1993; Anctil et al. 1994; Donelan et al. 1997).

Alternatively, the inertial dissipation (ID) method has been in relatively common usage for the measurements of fluxes from ships for almost 20 years (Large and Pond 1981). Here, the motion of the platform can be neglected because the ID method uses measured velocities only in the ''inertial subrange,'' at scales much smaller than, and independent of, those experienced by the ship. The ID method is based on an assumed balance between the production and dissipation of turbulent kinetic energy. Traditionally, the transport and pressure working terms are neglected, or assumed to be in balance (Large and Pond 1981). Recently, however, it has been suggested that the terms are not in balance, and several imbalance terms (functions of stability) have been proposed (Dupuis et al. 1995; Yelland and Taylor 1996). In a marine boundary layer, where some of the

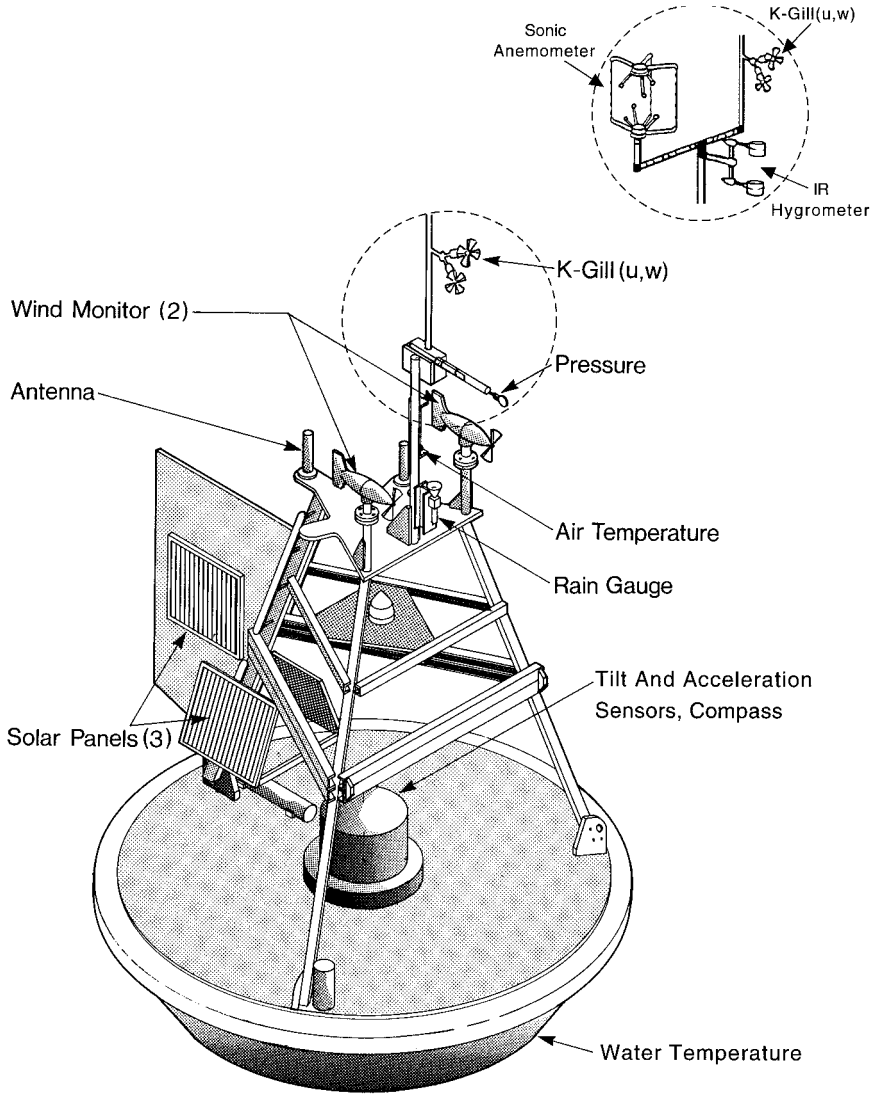

FIG. 2. NDBC 3-m discus wave directional buoy, showing SWADE and High-Res-II (inset) modifications.

stress may be supported by long (with respect to the measurement height) waves, the divergence of the energy transport and pressure working terms may be affected by the long-wave-supported energy flux and pressure working, and a simple dependence of the *sum* of these terms on stability only may not be appropriate. In addition to the above uncertainties, the ID method uses the Kolmogorov constant, whose value has an uncertainty of about $\pm 10\%$ (Edson et al. 1991). Hence, the ID method should be looked on as being approximate, and probably unsuitable for the study of the stress over the ocean in the presence of swell.

During SWADE, three NDBC 3-m discus buoys (Fig. 2) were deployed for continuous measurements of surface fluxes and directional wave spectra. In standard usage, the buoys are designed to measure the directional characteristics of waves, along with mean meteorological parameters. As such, they are equipped with a Datawell Hippy 40 sensor measuring heave, pitch, and roll; a triaxial magnetometer; two propeller anemometers; and sensors for air and water temperatures and atmospheric pressure (see Steele et al. 1992). In order to carry out the required direct (eddy correlation) measurements of the momentum flux, several modifications were made to the buoys (see Fig. 2). To complete the motion package, three orthogonally mounted linear accelerometers (two Sunstrand KA-1100s and a KA-1400) and a General Oceanics 6011TAMS axial fluxgate magnetometer were added, supplementing the Hippy 40. An onboard computer and optical WORM drives were added for continuous sampling and recording of the time series.

A K-Gill anemometer (Ataktürk and Katsaros 1989), with two propellers at $\pm 45°$ from the horizontal, was

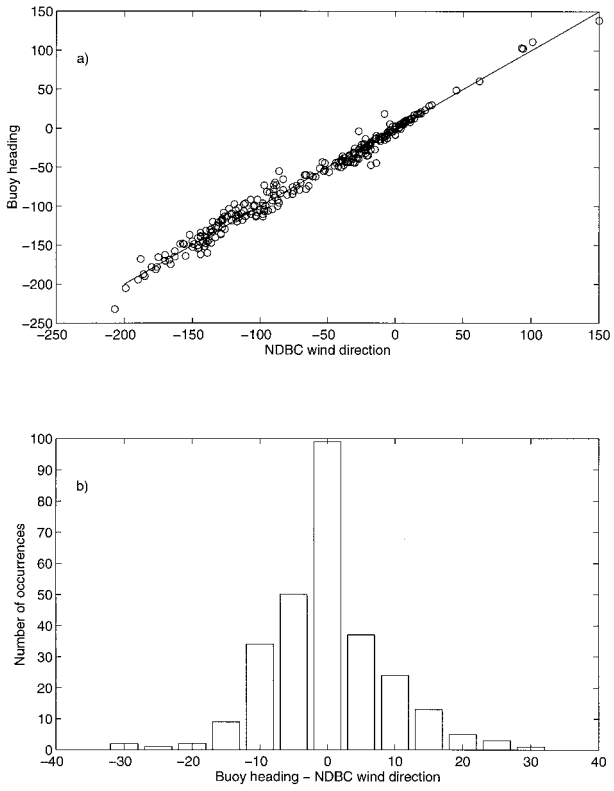

FIG. 3. (a) Buoy heading via magnetometer vs wind heading via NDBC propeller anemometer at 4 m for Discus-Centre data with $U > 4$ m s^{-1}. The solid line shows a 1:1 relationship; (b) histogram of difference between buoy heading and wind heading.

mounted at a height of 5 m above sea level. Although K-Gills are usually mounted with a vane to orient them into the wind, this configuration was avoided on the buoys so as to eliminate the possibility of the buoy exciting the vane thereby introducing spurious lateral wind fluctuations. Instead, the buoy itself was vaned and the K-Gill was mounted pointing toward the bow of the buoy, that is, away from the vane. In most conditions this ensured that the anemometer was pointed into the wind. In cases of light wind, however, friction in the mooring swivel may prevent proper heading. For this reason, all runs with mean wind speeds, U, under 4 m s^{-1} were omitted. This criterion was selected by comparison of the mean wind heading as obtained from the NDBC propeller vane at 4-m height with the mean buoy heading from the magnetometer. In Fig. 3, we show the comparison from the Discus-Centre dataset. The plot shows excellent agreement between the two headings, with one standard deviation corresponding to 8.6 degrees difference, and only 10 points out of 280 in excess of 20 degrees difference. The presence of strong currents, such as the Gulf Stream, results in additional forces on the mooring, which can degrade the vane's ability to keep the buoy pointed into the wind. To verify that this was not, in fact, a problem, comparisons between the buoy heading and NDBC wind direction were made for each buoy. Any data showing a systematic deviation between the two were removed from the dataset.

For each of the High-Res experiments in 1991 (High-Res-I) and 1993 (High-Res-II), two buoys were deployed with an additional near-surface three-axis ultrasonic current meter (water depth $\sim$ 10 m). The payload of the High-Res-II buoys was enhanced by the addition of a Solent three-axis sonic anemometer. The sonic and K-Gill were mounted at the same level, 2 m apart, symmetrically about the center point of the buoy (Fig. 2).

The procedure to produce motion-corrected wind velocity signals, given measured wind velocities and platform motion, is outlined in Anctil et al. (1994). We summarize the steps involved here:

- Removal from K-Gill dataset of all runs with either $U < 4$ m s^{-1} or min(u) < 2 m s^{-1}, the latter condition set so as to avoid possible stalling of the propeller.
- Correction for frequency response of K-Gill propellers following Hicks (1972). The distance constant for the carbon fiber propellers was determined to be 2.2 m.
- Computation of the velocity components in the anemometer reference frame, following Ataktürk and Katsaros (1989).
- Computation of the velocity components in an earth-referenced (ER) frame, following Anctil et al. (1994). The calculation, performed at each time step, consists of (i) rotating the measured velocities into an ER frame, (ii) adding the ER velocity fluctuations of the buoy itself, and (iii) accounting for the relative motion between the buoy (motion package) and anemometer. Note that with a K-Gill or other 2D anemometer the rotation (i) is not complete, due to missing crosswind (v component) information.
- Rotation of the ER horizontal and vertical velocities (u and w) so that $\overline{w} = 0$.
- Correction of cospectrum, S_{uw}, to account for missing high-frequency contributions (due to low sampling rate), using the universal curve of Miyake et al. (1970b).
- Correction of u_* to surface values, following Donelan (1990).

In Fig. 4, we show sample horizontal in-line and vertical velocity spectra along with a S_{uw} cospectrum. The universal curve of Miyake et al. (1970b) is also shown. This example is from the High-Res-II buoy, where the data were sampled at 4 Hz. In this case, the data cover the entire flux-carrying frequency range, and the universal curve correction is negligible. For the SWADE data, with sampling rates limited to 1 Hz due to storage considerations, corrections are typically in the range of 1%–20% (Anctil et al. 1994), with correction increasing with wind speed. With the greatly increased storage capacity available today, higher sampling rates have eliminated the need for the universal curve correction.

The addition of the sonic anemometer removes the minimum wind speed criterion and allows for estimation

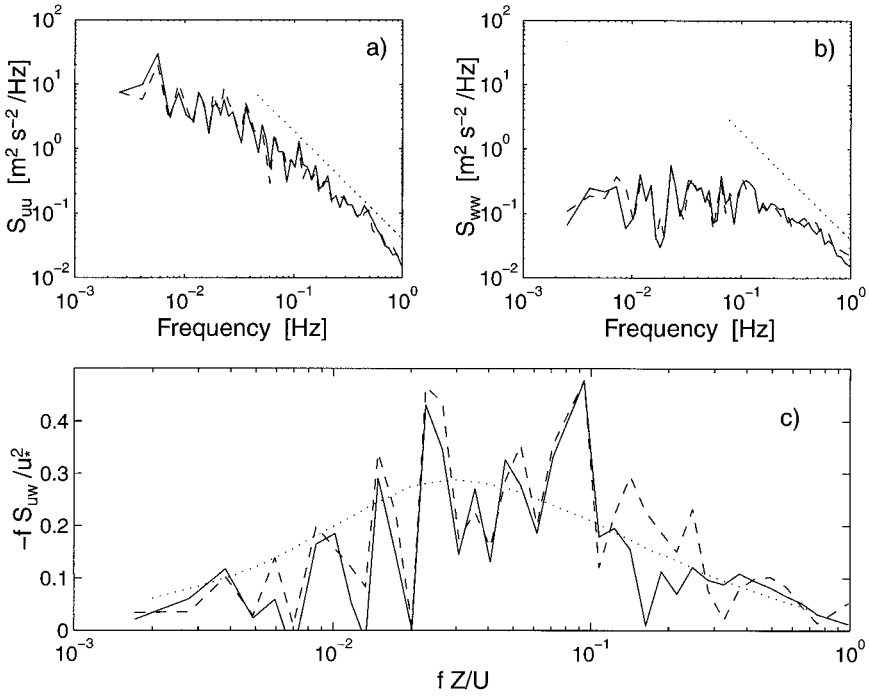

FIG. 4. Comparison of spectra of the wind velocities. Data are from buoy High-Res-II, at 0915 UTC 29 May 1993, sampled at 4 Hz using the K-Gill (solid line) and sonic (dashed line) anemometers. (a) and (b) Horizontal (in-line) and vertical velocity spectra, respectively, with the inertial subrange slope designated with a dotted line; (c) the normalized *u*–*w* cospectrum, with the proposed universal curve of Miyake et al. (1970b) shown by the dotted line; *Z* and *U* are the height above the surface and the mean velocity, respectively.

of stress at any wind speed. However, the bow of the buoy must point within $\pm 90°$ into the wind so as to avoid possible interference from the struts of the asymmetric sonic head. With all three components of the wind vector measured, the sonic can be used to measure the full stress vector [cf. Eq. (2)]. In contrast, the K-Gill, measuring only two components of the wind, measures only the component of the wind stress vector in line with the wind (i.e., $-\overline{u'w'}$, not $-\overline{v'w'}$). We comment further on this below. In Fig. 4 we plot sonic horizontal and vertical velocity spectra plus the cospectrum S_{uw} from the same period as the K-Gill data. To conserve power, the sonic was operated for only one-third the time of the K-Gill and ceased operation after eight days.

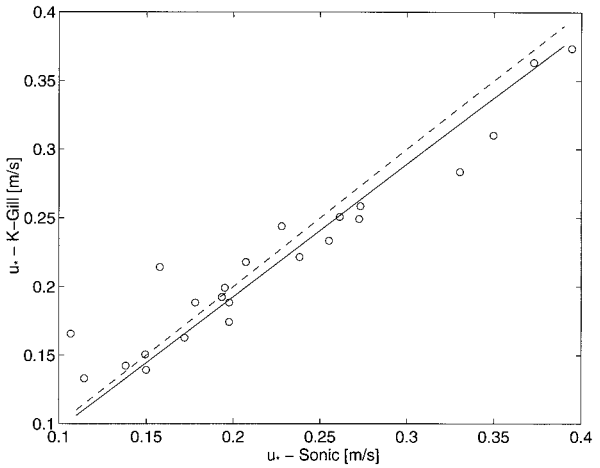

FIG. 5. Comparison of friction velocities as computed from the sonic and K-Gill anemometers using all 23 cases with $U > 4$ m s^{-1}. The lines are 1:1 (dashed) and best linear fit with constraint of zero offset (solid).

In Fig. 5, we plot friction velocities as determined from the K-Gill and Solent sonic for cases where $U > 4$ m s^{-1}. For the comparison, the horizontal component of the sonic wind has not been rotated into the mean wind direction, but is rather the component in line with the vane, since that is the component measured by the K-Gill. Constraining the offset to be zero and using a symmetrical maximum likelihood regression, the slope with 95% confidence limits is 0.96 ± 0.15. Hence we conclude that the K-Gill accurately yields the in-line component of the stress.

In Fig. 6a, we plot the angle of the mean sonic wind vector with respect to the buoy bow. For wind speeds above 4 m s^{-1}, the vane of the buoy keeps the buoy pointed within $\pm 6.8°$ (1 std dev) of the mean wind. This is in agreement with our earlier comparisons of buoy heading with NDBC wind heading (Fig. 3). At lower wind speeds, the heading deviation increases significantly, supporting our criterion that $U > 4$ m s^{-1} for K-Gill stress data to be accepted.

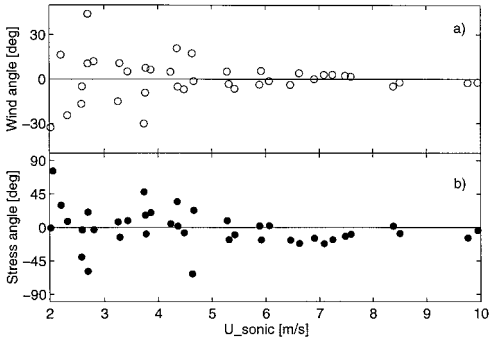

FIG. 6. High-Res-II sonic data: (a) mean angle of wind with respect to buoy bow versus mean wind speed; (b) mean angle of wind stress with respect to mean wind direction vs mean wind speed.

The angle of the stress vector with respect to the mean wind direction is plotted against mean wind speed and time in Figs. 6b and 7b, respectively. For wind speeds above 4.7 m s^{-1} the measured total stress deviates from the stress component in line with the wind by less that 22°. The expected stress underestimation by the K-Gill is thus less than 8%. Hence we expect the scalar stress and drag coefficient measured by the K-Gill (where $U > 4$ m s^{-1}) to be generally close to the true vector values, except perhaps in conditions of strong swell (e.g., Rieder 1997) or rapidly turning winds (Geernaert et al. 1986) where the difference between wind and stress vectors may exceed 22°. We note here that any such error would lead to an underestimate of stress in conditions of swell and would therefore enhance the effects discussed below. Although the sonic anemometer data serve to validate the K-Gill measurements, there are insufficient data to draw any conclusions related to stress angle (Figs. 6 and 7).

3. Estimating directional spectra

NDBC 3-m discus buoys are designed to produce average directional wave information, based on 17 minutes sampling, each hour. The results are output in the form of the heave–pitch–roll (HPR) cross-power spectral density (CPSD) matrices and direction coefficients following Longuet-Higgins et al. (1963). During SWADE and High-Res, wave data were sampled continuously and stored onboard for subsequent processing.

The accuracy of HPR buoy spectra depends critically on how well the buoy responds to the surface slopes. Kuik et al. (1988) showed that noise levels of 5% in slope can lead to errors of 30% in the directional width of the estimated spectra. NDBC has carried out thorough analyses of the performance characteristics of their buoys and incorporated hull correction factors into the reported directional parameters—see Steele et al. (1985) and Steele et al. (1992). In the energy containing range (0.05–0.3 Hz), it is assumed that the buoy motion follows linear theory, which implies that

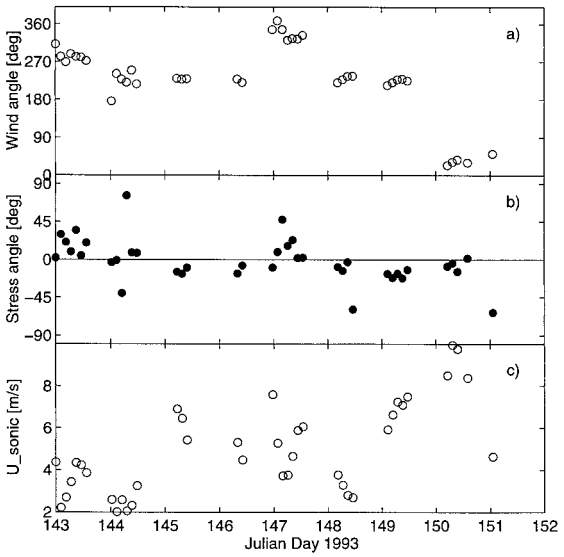

FIG. 7. High-Res-II sonic data: (a) mean wind heading vs time; (b) mean angle of wind stress relative to the wind direction vs time; (c) mean wind speed vs time.

$$C_{11}k^2 = C_{22} + C_{33} \quad \text{and} \quad C_{13} = C_{23} = 0, \quad (5)$$

where $C = C_{lm} + iQ_{lm}$, a function of frequency, is the CPSD matrix, and C_{lm} and Q_{lm} are the real and imaginary parts (co- and quad-) of the cross spectrum between the lth and mth channels. Here subscripts 1, 2, and 3 refer to heave displacement, pitch, and roll, respectively, and k is the wavenumber corresponding to the appropriate frequency.

In general, however, the response of the hull results in a deviation from the above. NDBC suggests correcting the coefficients in order to satisfy the above conditions. Having done this, we carry out the directional analysis of the time series using the maximum likelihood method (MLM) of Capon (1969). MLM, originally developed for analyzing seismic data, has been extended by Isobe et al. (1984) to deal with ocean wave data from a variety of sensors including heave–pitch–roll buoys. From an array of three sensors, the 3 × 3 CPSD matrix among the various signals is calculated. The ML estimate of the directional energy distribution at a given frequency ω_m and wave direction θ_l is then given by

$$S(\omega_m, \theta_l) = \Lambda[\mathbf{H}(\omega_m, \theta_l)^{*\mathrm{T}} C^{-1}(\omega_m)\mathbf{H}(\omega_m, \theta_l)]^{-1}, \quad (6)$$

where C represents the 3 × 3 CPSD matrix at frequency ω_m, and H the 3 × 1 array of complex phase information for the three signals. Here T and ∗ represent the matrix operations transpose and conjugate, respectively, and Λ is a normalizing factor defined so that the integrated total energy is equal to the average energy of the one-dimensional spectra.

In general, H takes into account that instruments may not be collocated, resulting in a phase shift between signals, or that different instruments (e.g., a collocated

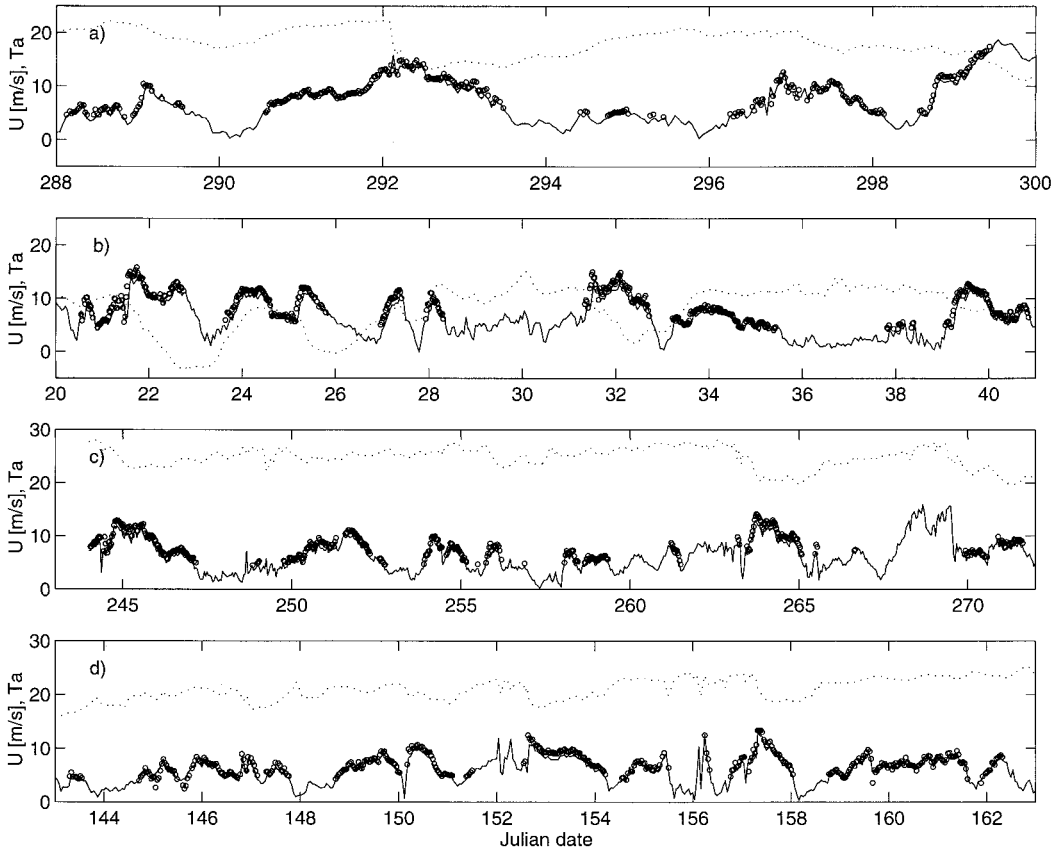

FIG. 8. Mean meteorological conditions measured on (a) SWADE-Discus North (1990), (b) SWADE-Discus Centre (1991), (c) High-Res-I HiRes-East (1991), and (d) High-Res-II HiRes-West (1993). The solid and dotted lines are wind speed and air temperature, respectively. Circles show 5-m winds during times of collection of stress data.

wave staff and current meter) may produce signals that are not in phase. For HPR data, Isobe et al. show that $\mathbf{H} = (1, -i\cos\theta_l, -i\sin\theta_l)$. We note that the above analysis can be carried out on either the HPR time series or the CPSD matrices produced by NDBC analysis.

4. The data

During SWADE two modified NDBC 3-m discus buoys were deployed off the coast of Virginia in October 1990 for the 6-month experiment. A third buoy was added in January 1991. These buoys were designated Discus-North, Discus-East, and Discus-Centre (Fig. 1).

Throughout the period, the buoys provided mean meteorological and directional wave data in their role as NDBC buoys. In other words, the data were processed onboard and transmitted to shore following standard NDBC protocol. The calculated cross-spectral density coefficients were further processed using the MLM, as discussed above. Directional spectra at 3-h intervals during the October 1990 Intensive Operating Period 1 (IOP1) and February–March 1991 (IOP3) are found in Caruso et al. (1993, 1994).

K-Gill anemometers and ''cans'' containing the translational accelerometers and onboard storage devices were installed on discus buoys at various times. In particular, flux data were collected at Discus-North and -Centre during October 1990 and January–February 1991, respectively. Meteorological conditions during October 1990 were dominated by a series of three storms, which passed through the SWADE area at the end of the month (see Fig. 8a). The so-called SWADE storm of 26 October (Julian day 299) was one of the largest to hit the area in recent years (Cardone et al. 1995), and the recorded data include winds of 18 m s^{-1} and waves of 6 m significant height. During its 20 days of recording, Discus-C experienced conditions typical of the area in winter, with alternating air masses of cold, dry continental air and warm, humid southern air (see Fig. 8b).

Six months after the end of the SWADE campaign, the cans were again deployed on two buoys during the High-Res experiment off North Carolina. One of the High-Res-I buoys was positioned well inside the Gulf Stream, while the other one was on the shelf off Cape Hatteras. Meteorological conditions experienced during High-Res-I are summarized in Fig. 8c: winds were gen-

TABLE 1. Discus buoys with flux measurements during SWADE and High-Res.

Buoy	WMO number	Location	Depth (m)	Period	S_f (Hz)	Data
Discus-N	44001	38°22.1′N, 73°38.9′W	115	90.10.10–90.10.28	1	312
Discus-C	44023	37°32.1′N, 74°23.5′W	102	91.01.20–91.02.08	1	485
Hi-Res-E	44026	36°00.0′N, 73°20.0′W	3307	91.09.01–91.09.30	2	445
Hi-Res-W	41017	35°25.0′N, 75°15.0′W	33	93.05.22–93.06.12	4	408

erally light–moderate and variable with several moderately intense events.

Finally, during spring 1993, the cans were again deployed for High-Res-II, yielding stress data in the nearshore shelf regime. Meteorological conditions during this period were similar to those of High-Res-I: generally light–moderate winds with the passage of several moderate systems. The wave field during High-Res-II was dominated by swells, typically propagating perpendicular to the wind sea. Figure 8 and Table 1 summarize the successful data collection periods of the flux measurements.

In Fig. 9, we plot the 10-m neutral drag coefficients for each of the four buoys, using the profile relations of Donelan (1990) to convert the measured 5-m wind speeds to neutral 10-m values. It is evident that an attempt to determine a relationship between drag coefficient and wind speed is made difficult not only by scatter within each dataset but also by differences between datasets. Such scatter is usual among similar flux datasets. We investigate here whether some of the scatter can be attributed to specific geophysical conditions.

Given the additional uncertainty in the Discus-North and -Centre data due to lower sampling rates, we focus attention on the High-Res results. High-Res-I data are replotted in Fig. 10. Here, two events (time sequences

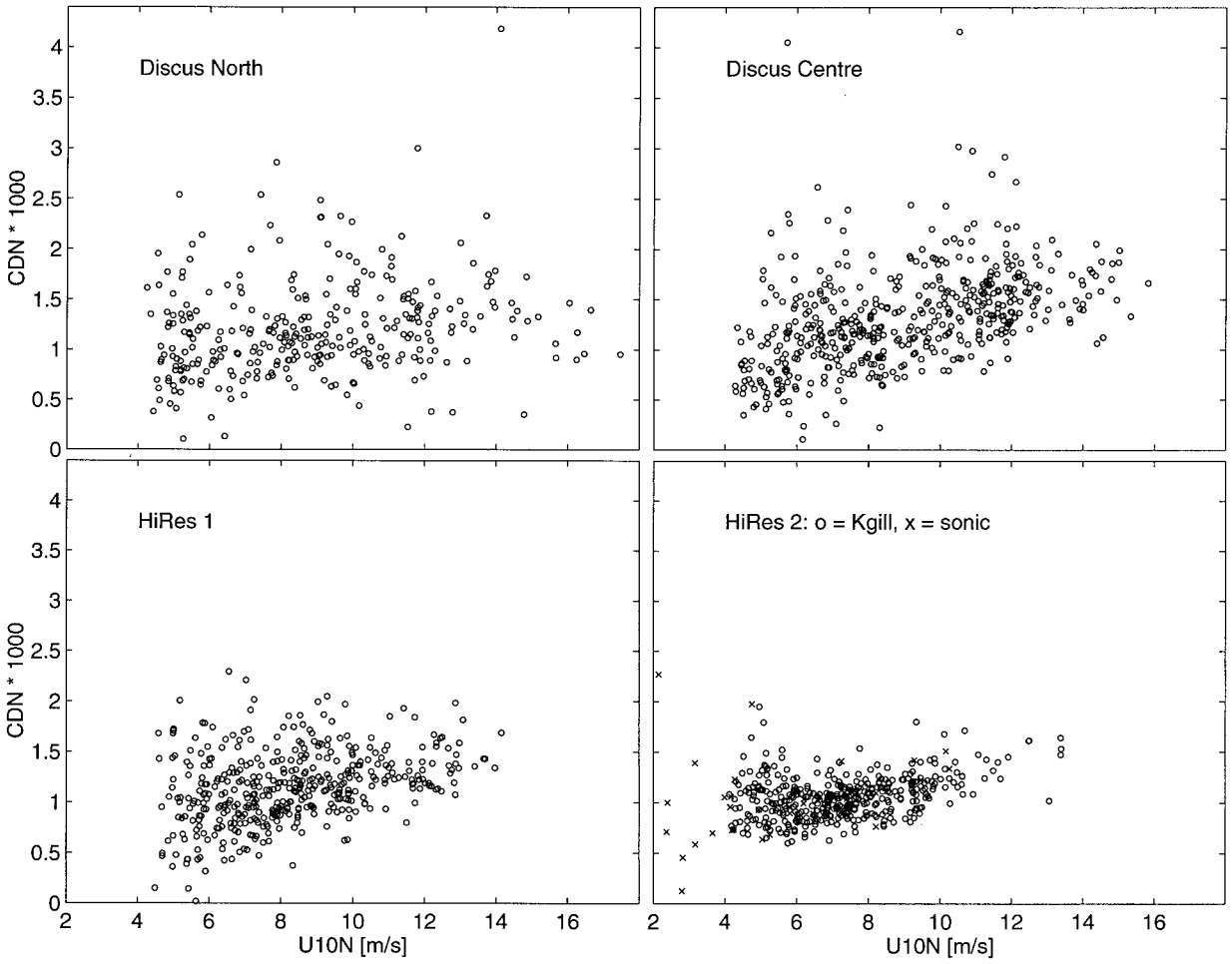

FIG. 9. Neutral drag coefficients at 10 m C_{10N} vs 10-m neutral wind speeds U_{10N} for Discus North, Discus Centre, High-Res-I, and High-Res-II.

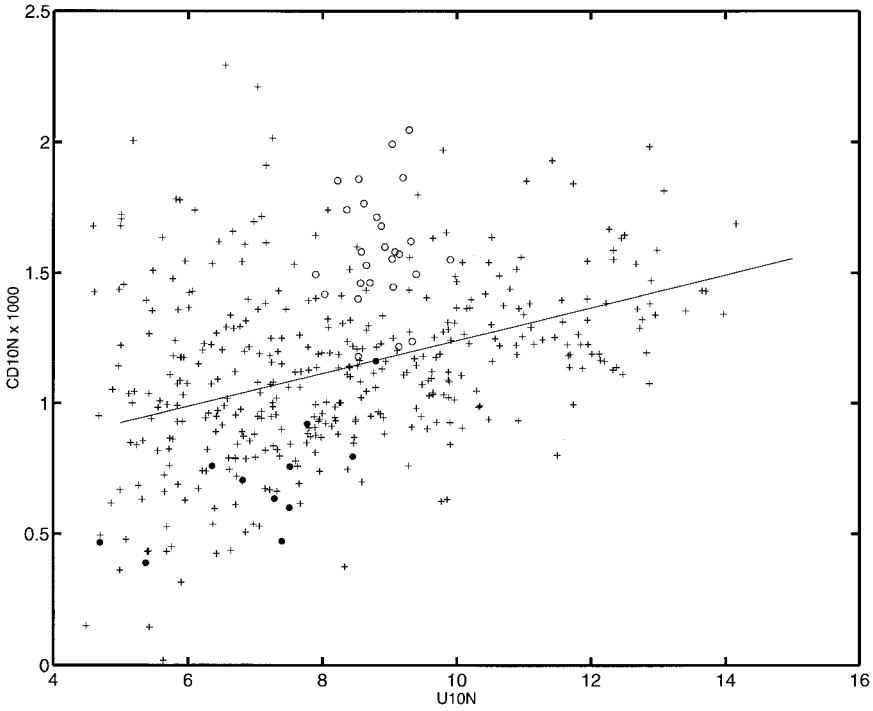

FIG. 10. Ten-meter neutral drag coefficients, C_{10N} vs 10-m neutral wind speeds U_{10N} for High-Res-1. The solid and open circles represent continuous time series during JD 261 and 270–271, respectively. The line represents the relation of Smith (1980).

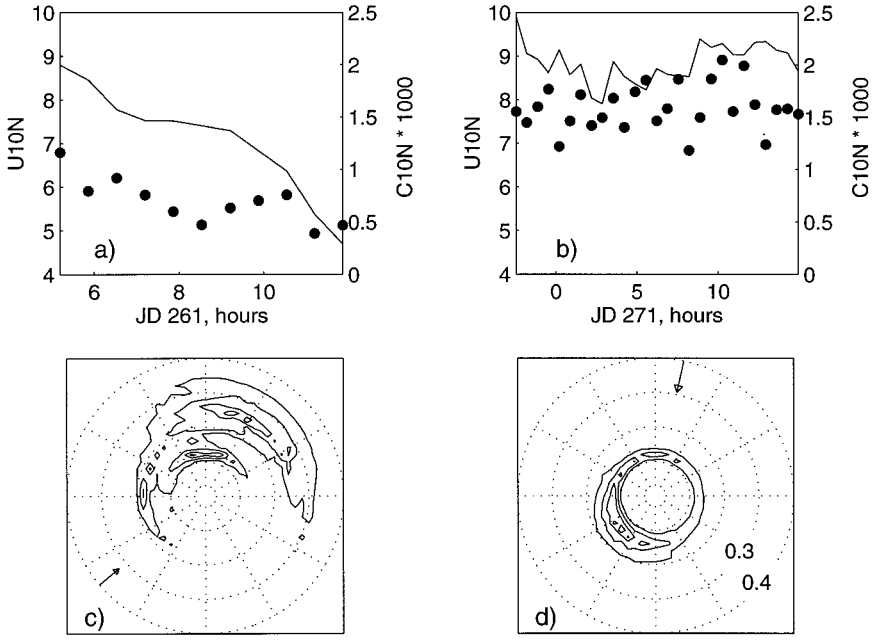

FIG. 11. (a) Wind speed U_{10N} (solid line) and 1000× drag coefficient C_{10N} (circles) during 1991 JD 261; (b) as (a) during JD 271; (c) directional wave spectrum around 08:45 UTC, JD 261. Grid lines are 30° apart, with frequencies every 0.1 Hz to a maximum of 0.4 Hz. North appears at the top of the plot, east at the right. The wave energy is shown in the direction of propagation, with equally spaced contours normalized to the energy maximum. The mean wind from the K-Gill anemometer is represented by an arrow pointing in the direction of the wind, with an arrow of length equal to the 0.1-Hz spacing equivalent to a wind speed of 10 m s^{-1}; (d) as (c) for 23:30 UTC JD 270.

of data) have been identified and distinguished on the plot. The filled circles were measured in a decaying (and turning) wind on Julian day (JD) 261, 1991—see Fig. 11a. A typical directional spectrum from this period (Fig. 11c) shows a confused sea with cross/following swell; $H_s = 0.95$ m. Here the measured drag coefficients are low, $\overline{C_{10N}} = (0.7 \pm 0.13) \times 10^{-3}$, where the uncertainty corresponds to twice the standard error. This error includes variability in C_{10N} due to the change in wind speed during the event. If we account for this latter effect using, say, the wind speed dependence of the Smith (1980) drag coefficient relation we find $\overline{C_{10N}} = (0.7 \pm 0.1) \times 10^{-3}$, where the error is now a measure of the statistical uncertainty alone of the measurement. We note that C_{10N} for the event is significantly lower (at a 95% confidence level) than that of the remaining dataset or the predictions of Smith (1980) or Yelland and Taylor (1996). It is unclear whether this difference is due primarily to the presence of following swells, the decay of the wind field, or both. Situations of this complexity dominate the dataset, making it difficult to isolate effects.

A second event, marked with open circles on Fig. 10, is distinguished by higher than typical drag coefficients, $\overline{C_{10N}} = (1.6 \pm 0.1) \times 10^{-3}$, again showing the statistical uncertainty of the measurement. For comparison, the Smith (1980) relation predicts $C_{10N} = 1.17 \times 10^{-3}$ at this mean wind speed. During this event, a 17-h period on 1991 JD270-271, the wind was relatively steady, around 9 m s^{-1}, from the north (Fig. 11b). A directional wave spectrum from 2330 UTC JD 270 shows two wave fields: the dominant windsea ($f_p = 0.14$ Hz) and a smaller, but still significant, swell, with $f_p = 0.12$ Hz, traveling against the wind (Fig. 11d). This swell is the remnant of a 40-h storm on JD 267-268 with southerly winds up to 16 m s^{-1} and waves to $H_s = 4.2$ m. It is likely that the higher drag coefficients observed during JD270–271 are due to the presence of the counterswell (cf. Donelan et al. 1997). If we now consider all High-Res-I counterswell cases with steady or increasing wind, C_{10N} was found to be enhanced by about 25% above the remaining population—significant at the 95% confidence level. Similarly, the counterswell drag coefficients were enhanced significantly (95%) over both the Smith (1980) and Yelland and Taylor (1996) relations. The same analysis was carried out on the High-Res-II dataset. The wave field during this campaign was dominated by cross swells, and the drag coefficients showed less scatter compared to the High-Res-I data (see Fig. 9). Again, drag coefficients measured in the presence of counterswells were found to be enhanced over the remaining data, but the significance is lower due to the small number of cases (22, over the wind speed range 4.5–13.5 m s^{-1}).

The task of determining a drag coefficient–wind speed relationship is simplified by restricting the dataset to pure windsea cases. To identify these cases, the directional spectra were analyzed using wave partitioning

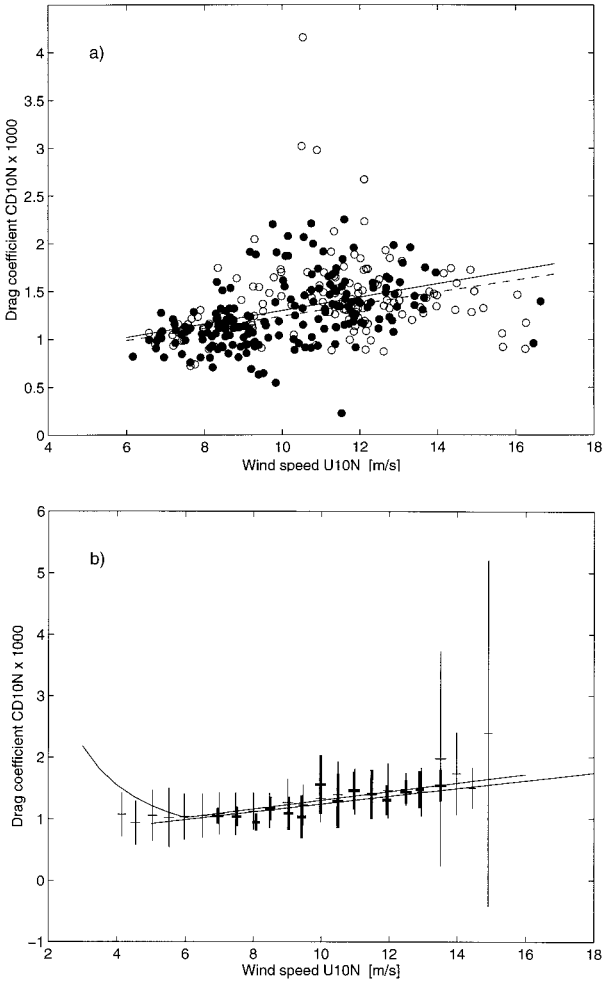

FIG. 12. (a) Ten-meter neutral drag coefficients, C_{10N} vs 10-m neutral wind speeds U_{10N} for pure wind sea cases, all buoys. The filled circles indicate data taken in stationary conditions; the open circles in nonstationary conditions. The curves are Yell and Taylor (1996) (solid) and Smith (1980) (dashed). (b) C_{10N} vs U_{10N} in bins of 0.5 m s^{-1}. The thick and thin lines represent one standard deviation of the stationary pure windsea data subset and the full dataset, respectively.

(Kline and Hansen 1995), which enables systems to be identified and tracked. Over three-quarters of the full dataset, including almost all points with $U_{10N} < 6$ m s^{-1}, is eliminated by excluding conditions of swell or mixed sea states. The remaining data (all buoys) are plotted in Fig. 12a. A fit to all data points with $6 < U_{10N} < 14$ m s^{-1} yields

$$1000C_{10N} = 0.07U_{10N} + 0.60. \quad (7)$$

The coefficients also describe (to within 3%) the best fit to the full dataset in this range. The same drag relation was reported by Yelland and Taylor (1996) to describe their extensive Southern Ocean inertial dissipation dataset in the range $U_{10N} > 6$ m s^{-1}.

Finally, we comment that the scatter in the reduced dataset, although much diminished, is still significant.

Again, we claim that some of the scatter can be attributed to known geophysical events. For instance, high drag coefficients from Discus-Centre for $U_{10N} \approx 11$ m s^{-1} occur during a period when conditions were strongly nonstationary. If we additionally exclude nonstationary cases [those where hourly changes (four-hourly trends) are greater than 1 m s^{-1}/h (0.5 m s^{-1}/h) in wind speed or 20°/h (10°/h) in direction], only 186 runs, 11% of the total dataset, remain; these appear as solid circles in Fig. 12a. In Fig. 12b, we plot the means of the drag coefficients in 0.5-m wind speed bins of both the stationary, pure windsea dataset and the full dataset. The thick and thin lines represent one standard deviation of the subset and full set, respectively. It is seen that the scatter is generally reduced, often considerably, despite the great (order of magnitude) reduction in the number of points. This is consistent with Donelan et al. (1997), whose pure windsea (steady) drag coefficients showed considerably less scatter than those taken in mixed seas.

5. Discussion and conclusions

The question of a possible sea state dependence on the drag coefficient has received a lot of attention recently. The dependence of C_{10N} on wave age for pure windseas has now been established, at least qualitatively (and after considerable controversy), but in the open ocean where the variation in wave age is small, this is of secondary importance. The open ocean is dominated by swells, and how these influence the drag coefficient has not yet been established. Evidence to date has been contradictory.

Yelland and Taylor (1996) in their analysis of shipborne inertial dissipation stress data from the southern oceans did not find a significant sea state dependence; they concluded that ''the effects of sea state on wind stress may not be as large or frequent as sometimes suggested.'' We note, however, that their wave measurements are limited to H_s, with no frequency or directional information. Hence their analysis of sea state effects was severely compromised.

Dobson et al. (1994) presented shipborne ID data in conditions of strong swells and tested the hypothesis that truncating the one-dimensional wave spectra to eliminate swells would change existing drag coefficient–wave age relations. Although the significance was low, their data did not support the hypothesis of a sea state effect. Their conclusions recommend a reevaluation of the problem using two-dimensional spectra.

Rieder (1997) recently presented a set of eddy-correlation stress data from the moored platform *FLIP*, in the open ocean off California. In analyzing the drag coefficient, he found large temporal variability occurring over timescales of hours to days. This corroborates our findings here, implying geophysical variability in the data. However, a multivariate analysis of C_{10N} in terms of wave age and H_s was able to account for only 28% of the variability. His work identified wind field nonstationarity, in particular turning winds, as a likely candidate for some of the enhanced variability.

Donelan et al. (1997), with eddy-correlation stress and two-dimensional wave spectra data from a ship, found significantly enhanced drag coefficients in conditions of light winds and opposing swells, which they attributed to the presence of swells. They also pointed out that an inertial dissipation analysis of the same data did not result in the same enhancement. This is consistent with the results summarized above, with the two ID analyses finding no sea state effect on C_{10N}, and the eddy-correlation studies attributing some C_{10N} variability to sea state.

We have presented here an extensive (over 900 h) set of open ocean stress and wave data from discus buoys. In addition to being one of the largest sets of direct or eddy-correlation stress data, it is one of few with concurrent two-dimensional ocean wave spectra. The neutral drag coefficients were studied, and it was found that much of the scatter present in the drag coefficient versus wind speed relation could be attributed to two aspects of geophysical variability. Specifically, the presence of background swells and nonstationarities in the wind field can significantly affect the drag coefficient. The implications of this are that the long-sought simple parameterization of drag coefficient on wind speed alone is not realizable.

If the effects of sea state on drag are to be properly parameterized, further experimental work must be done. The open ocean is characterized by windseas and swells of varying magnitude and direction, along with winds both steady and changing. Of the open ocean data presented here, only 11% fall into the ideal category of stationary winds and pure windsea. Often, conditions included rapidly changing winds blowing over a region of one or more swells propagating in different directions. Only through a long-term measurement program (including simultaneous eddy-correlation stress and directional wave measurements) covering a wide range of external conditions in the open ocean can we hope to isolate the various effects.

Acknowledgments. The authors gratefully acknowledge the support for SWADE provided by the U.S. Office of Naval Research through Grants N0014-1-0015, N0014-94-1-0629 and N0014-88-J-1028 to the National Water Research Institute (MAD and WMD) and N00014-90-J-1464 and N00014-92-J-1546 to the University of Miami (HCG) and for High-Res through Grant N0014-91-J-1775 to the University of Miami (HCG). We also acknowledge the assistance of the following people: Roland Desrosiers, Joe Gabriele, and Harry Savile of the National Water Research Institute designed, built, and maintained the onboard real-time recording systems on the discus buoys; the personnel of the National Data Buoy Center, especially Kenneth Steele, David Wang, Ed Michelena, Lloyd Ladner, Bill Beacht, Jim Patterson, David Wittorf, and Capt. Ted Colburn

provided support during all phases of the field experiment; John Kemp and John Bouthillette of WHOI, and the crew of the R/V *Oceanus* provided support during the deployment and recovery phases of the buoys as well as during several maintenance cruises. Finally, we thank the reviewers for their constructive comments.

REFERENCES

Anctil, F., M. A. Donelan, W. M. Drennan, and H. C. Graber, 1994: Eddy correlation measurements of air–sea fluxes from a discus buoy. *J. Atmos. Oceanic Technol.*, **11,** 1144–1150.

Ataktürk, S. S., and K. B. Katsaros, 1989: The K-Gill: A twin propeller-vane anemometer for measurements of atmospheric turbulence. *J. Atmos. Oceanic Technol.,* **6,** 509–515.

Bradely, E. F., P. A. Coppin, and J. S. Godfrey, 1991: Measurements of sensible and latent heat flux in the western equatorial Pacific Ocean. *J. Geophys. Res.,* **96,** 3375–3389.

Capon, J., 1969: High-resolution frequency-wavenumber spectrum analysis. *Proc. IEEE,* **57,** 1408–1418.

Cardone, V. J., H. C. Graber, R. E. Jensen, S. Hasselmann, and M. J. Caruso, 1995: In search of the true surface wind field in SWADE IOP-1: Ocean wave modelling perspective. *Global Atmos. Ocean Sys.,* **3,** 107–150.

Caruso, M. J., H. C. Graber, R. E. Jensen, and M. A. Donelan, 1993: Observations and modelling of winds and waves during the Surface Wave Dynamics Experiment. Report 1—Intensive observation period IOP-1, 20–31 October 1990. Tech. Rep. CERC-93-6, 206 pp. [Available from U.S. Army Corps of Engineers, Washington, DC 20314.]

——, ——, ——, and ——, 1994: Observations and modelling of winds and waves during the Surface Wave Dynamics Experiment. Report 2—Intensive observation period IOP-3, 25 February–9 March 1991. Tech. Rep. CERC-93-6, 294 pp. [Available from U.S. Army Corps of Engineers, Washington, DC 20314.]

Dobson, F. W., S. D. Smith, and R. J. Anderson, 1994: Measuring the relationship between wind stress and sea state in the open ocean in the presence of swell. *Atmos.–Ocean,* **32,** 237–256.

Donelan, M. A., 1987: The effect of swell on the growth of wind waves. *Johns Hopkins APL Tech. Digest,* **8,** 18–23.

——, 1990: *Air–Sea Interaction. The Sea*, Vol. 9. *Ocean Engineering Science,* B. LeMéhauté and D. Hanes, Eds., John Wiley and Sons, 239–292.

——, M. Skafel, H. Graber, P. Liu, D. Schwab, and S. Venkatesh, 1992: On the growth rate of wind-generated waves. *Atmos.–Ocean,* **30,** 457–478.

——, W. M. Drennan, and K. B. Katsaros, 1997: The air–sea momentum flux in mixed wind sea and swell conditions. *J. Phys. Oceanogr.,* **27,** 2087–2099.

Dupuis, H., A. Weill, K. B. Katsaros, and P. K. Taylor, 1995: Turbulent heat fluxes by profile and inertial dissipation methods: Analysis of the atmospheric surface layer from shipboard measurements during the SOFIA/ASTEX and SEMAPHORE experiments. *Ann. Geophys.,* **13,** 1065–1074.

Edson, J. B., C. W. Fairall, P. G. Mestayer, and S. E. Larsen, 1991: A study of the inertial-dissipation method for computing air–sea fluxes. *J. Geophys. Res.,* **96,** 10 689–10 711.

Fujitani, T., 1985: Method of turbulent flux measurement on a ship by using a stable platform system. *Pap. Meteor. Geophys.,* **36,** 157–170.

Geernaert, G. L., 1990: Bulk parameterization for the wind stress and heat fluxes. *Surface Waves and Fluxes,* G. L. Geernaert and W. J. Plant, Eds., Kluwer, 91–172.

——, K. B. Katsaros, and K. Richter, 1986: Variations of the drag coefficient and its dependence on sea state. *J. Geophys. Res.,* **91,** 7667–7679.

Hicks, B. B., 1972: Propeller anemometers as sensors of atmospheric turbulence. *Bound.-Layer Meteor.,* **3,** 214–228.

Isobe, M., K. Kondo, and K. Horikawa, 1984: Extension of MLM for estimating directional wave spectrum. *Proc. Symp. on Description and Modelling of Directional Seas,* Lyngby, Denmark, Danish Hydraulic Institute, A-6-1–A-6-15.

Katsaros, K. B., M. A. Donelan, and W. M. Drennan, 1993: Flux measurements from a Swath ship in SWADE. *J. Mar. Sys.,* **4,** 117–132.

Kitaigorodskii, S. A., and Y. A. Volkov, 1965: On the roughness parameter of the sea surface and the calculation of momentum flux in the near-water layer of the atmosphere. *Izv. Atmos. Oceanic Phys.,* **1,** 973–988.

Kline, S. A., and J. L. Hansen, 1995: Wave identification and tracking system. Tech. Rep. STD-R-2436, 39 pp. [Available from Johns Hopkins University, Applied Physics Laboratory, Laurel, MD 20723-6099.]

Kuik, A. J., G. Ph. van Vledder, and L. H. Holthuijsen, 1988: A method for the routine analysis of pitch-and-roll buoy wave data. *J. Phys. Oceanogr.,* **18,** 1020–1034.

Large, W. G., and S. Pond, 1981: Open ocean momentum flux measurements in moderate to strong winds. *J. Phys. Oceanogr.,* **11,** 324–336.

Longuet-Higgins, M. S., D. E. Cartwright, and N. D. Smith, 1963: Observations of the directional spectrum of sea waves using the motion of a floating buoy. *Ocean Wave Spectra,* Prentice-Hall, 111–132.

Mahrt, L., D. Vickers, J. Howell, J. Højstrup, J. M. Wilczak, J. Edson, and J. Hare, 1996: Sea surface drag coefficients in the Risø Air Sea Experiment. *J. Geophys. Res.,* **101,** 14 327–14 335.

Mitsuta, Y., and T. Fujitani, 1974: Direct measurement of turbulent fluxes on a cruising ship. *Bound.-Layer Meteor.,* **6,** 203–217.

Miyake, M., M. A. Donelan, and Y. Mitsuta, 1970a: Airborne measurements of turbulent fluxes. *J. Geophys. Res.,* **75,** 4506–4518.

——, R. W. Stewart, and R. W. Burling, 1970b: Spectra and cospectra of turbulence over water. *Quart. J. Roy. Meteor. Soc.,* **96,** 138–143.

Nghiem, S. V., and Coauthors, 1995: Observations on ocean radar backscatter Ku and C bands in the presence of large waves during the Surface Wave Dynamics Experiment. *IEEE Trans. Geosci. Remote Sens.,* **33,** 708–721.

Pierson, W. J., Jr, 1983: The measurement of synoptic scale wind over the ocean. *J. Geophys. Res.,* **88,** 1683–1708.

Rieder, K. F., 1997: Analysis of sea-surface drag parameterizations in open ocean conditions. *Bound.-Layer Meteor.,* **82,** 355–377.

Smith, S. D., 1980: Wind stress and heat flux over the ocean in gale force winds. *J. Phys. Oceanogr.,* **10,** 709–726.

——, and Coauthors, 1992: Sea surface wind stress and drag coefficients: The HEXOS results. *Bound.-Layer Meteor.,* **60,** 109–142.

Steele, K. E, J. C. Lau, and Y. L. Hsu, 1985: Theory and application of calibration techniques for an NDBC directional wave measurements buoy. *IEEE J. Ocean Eng.,* **OE-10,** 382–396.

——, C. Teng, and D. W. C. Wang, 1992: Wave directional measurements using pitch-roll buoys. *Ocean Eng.,* **19,** 347–375.

Yelland, M. J., and P. K. Taylor, 1996: Wind stress measurements from the open ocean. *J. Phys. Oceanogr.,* **26,** 541–558.